A New Current Phasor-Controlled ZVS Twin Half-Bridge High-Frequency Resonant Inverter for Induction Heating

Tomokazu Mishima, *Member, IEEE,* Chikanori Takami, *Non-Member, IEEE*, and Mutsuo Nakaoka, *Member, IEEE*

***Abstract*—A novel soft-switching high-frequency (HF) resonant (HF-R) inverter for induction heating (IH) applications is presented in this paper. By adopting the current phasor control of changing a phase shift (PS) angle between two half-bridge inverter units, the IH load resonant current can be regulated continuously under the condition of wide range soft-switching operations. In addition to this, the dual mode power regulation scheme based PS angle control & asymmetrical pulse-width-modulation (PWM) in one inverter unit is proposed for improving the efficiency in low output power settings. The essential performances on the output power regulation and soft-switching operations are demonstrated in an experiment using its 1 kW-60 kHz HF-R inverter prototype, then the topological validity is evaluated from a practical point of view.**

***Index Terms*—induction heating (IH), high-frequency (HF) resonant (HF-R) inverter, zero voltage soft-switching (ZVS), current phasor, phase shift (PS) angle control, asymmetrical PWM.**

I. Introduction

IH has been applied widely in a variety of electric power conversion processing such as home appliances (IH cookers), fluid heating systems, induction hardening, and superheated steamer system owing to its unique and practicable properties of direct and local heating, high efficiency and safety.

As an example of up-to-date IH technologies, the developments of HF inverters for IH metallic pans/vessels fabricated from low resistivity and low permeability materials such as aluminum and copper are gathering much attention in pursuing for energy saving home appliances amid global warming preventions. This type of IH process demands HF inverters operating in high efficiency, higher switching frequency and minimized switching power losses [1]-[10].

In order to attain the reduction of switching loss, low Electro-Magnetic Interference (EMI) noise and high power density effectively, the introduction of soft-switching technologies is useful in the HF-R inverter. The soft-switching HF-R inverter which have been developed so far have attractive features such as the low cost and simple control schemes based on pulse-frequency-modulation (PFM) and PWM. However, the HF-R inverters controlled by PFM have the inherent technical issue, i.e. switching frequency limitation for the low–medium output power settings, thereby the wide range power regulation oh the IH load cannot be ensured [3]. In addition, improvement of power density cannot be expected in the asymmetrical half-bridge HF inverter without the complicated power regulation schemes [5][6], and so in the phase shift PWM (PS-PWM) full-bridge (FB) inverters [11]–[15] because of the narrow soft-switching range. In particular, the conventional ZVS PS-PWM FB HF inverter as depicted in Fig. 1 suffers from severe soft-switching limitation in the controlled-phase active switches under the condition of low output power settings. The dual half-bridge inverter suitable for the coupled working coils is proposed in [4], but performances on the soft switching operations are not clearly demonstrated. Therefore, improvement of the power density is a significantly technical challenge for those previous type HF inverters while constraining the switching frequency.

As a HF inverter operating with higher switching frequency conditions, the triplex resonant frequency (TRF) inverter has been developed for a 2 kW-60 kHz IH cooker as reported in [1]. The 60 kHz TRF inverter can be actually utilized without increasing the switching power losses by adopting one-third switching frequency 20 kHz. However, the drawback of the TRF HF inverter is that the fundamental component of the load resonant current is inherently eliminated and not transferred to the IH load. Accordingly, power conversion efficiency might deteriorate in the large and rated output power area, thereby high efficiency as performed in the commercial HF inverters can not be expected.

As a new solution for the technical problem, an innovative soft-switching HF-R inverter is proposed in this paper. In the HF-R inverter proposed herein, ZVS operations can be attained over the wide range of output power variations together with a seamless power regulation by varying the PS angle between the two instantaneous resonant currents of the half-bridge inverter units, which is named as ”current phasor control” in this research. Therefore, the soft-switching operations can be maintained even in the low output power conditions, consequently the reductions of switching power losses and EMI noises can be realized effectively for the wide-range output power setting. Moreover, the proposed HF-R inverter

Manuscript received December 29, 2012; revised March 14, 2013 and May 2, 2013; accepted June 9, 2013.

T. Mishima and C. Takami are with the Mechatronics Engineering Division, Graduate School of Maritime Science, Kobe University, Hyogo, Japan (e-mail: mishima@maritime.kobe-u.ac.jp).

M. Nakaoka is with The Electric Energy Saving Research Center, Kyungnam University, Republic of Korea, with the Electrical & Telecommunication Engineering Division, University of Malaya, Kuala Lumper, and a professor emeritus of the Graduate School of Science & Engineering, Yamaguchi University, Yamaguchi, Japan.

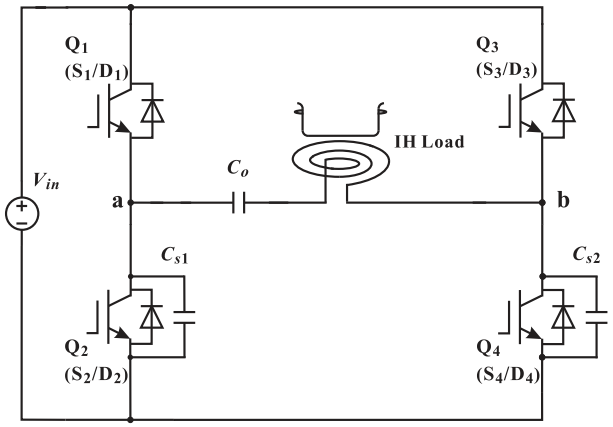

Fig. 1. Conventional ZVS PS-PWM FB HF inverter topology.

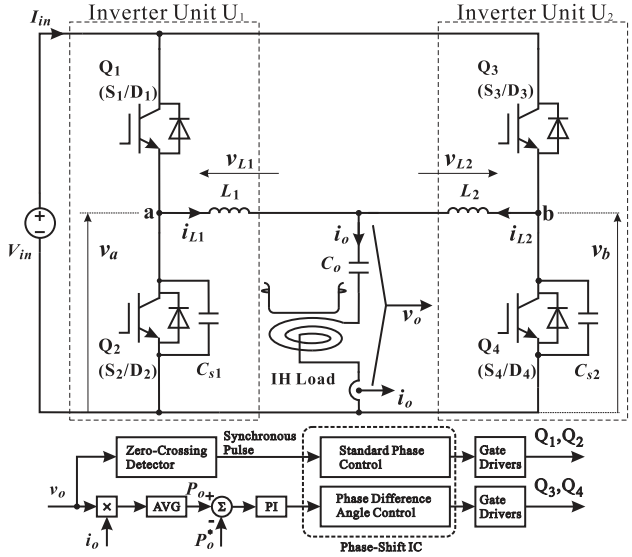

Fig. 2. A proposed current phasor-controlled ZVS HF-R inverter.

can operate as a single asymmetrical half-bridge inverter by exchanging the numbers of operating half-bridge inverter units. Thereby, high efficiency and high reliability power conversions can be expected in the low output power area of the proposed HF-R inverter.

This paper is presented for demonstrating and evaluating the soft-switching operations and steady-state power regulation characteristics of the newly-proposed soft-switching HF-R inverter in an experiment using a 1 kW-60 kHz prototype, then its practical effectiveness is originally clarified.

The remainder of this paper is organized as follows. The circuit configuration and its operation principle of the proposed ZVS HF-R inverter are described in Section II. An analysis of the output power regulation based on the current phasor control is demonstrated by using the simplified equivalent circuit of the proposed HF-R inverter in Section III. Then, the HF-R inverter characteristics of the wide-range power regulation are theoretically clarified in the same section. The experimental verifications on the soft-switching operation, wide-range and seamless power regulation are carried out by using the 1 kW-60 kHz prototype in Section IV. In addition to these, the validity of the dual-mode control scheme for improving the conversion efficiency in the low output power setting is actually evaluated in the experiment. Furthermore, performance comparison between a conventional ZVS PS-PWM FB HF inverter and the proposed HF-R inverter with the single and dual mode controls are demonstrated in terms of soft-switching range and conversion efficiency. Finally, the effectiveness of the proposed HF-R inverter is demonstrated from a practical point of view.

II. A New ZVS HF Resonant Inverter

A. Circuit Description

A schematic diagram of the proposed HF-R inverter is illustrated in Fig.2. The HF-R inverter treated herein is composed of the two asymmetrical half-bridge inverters U_1 and U_2 which share the IH load. The IH load which consist of the IH working coil and a metallic utensil (pan, vessel) are represented by the equivalent effective resistance R_o and equivalent effective inductance L_o. The resonant and power factor correction (PFC) tuned capacitor C_o is connected in series with the IH load [16].

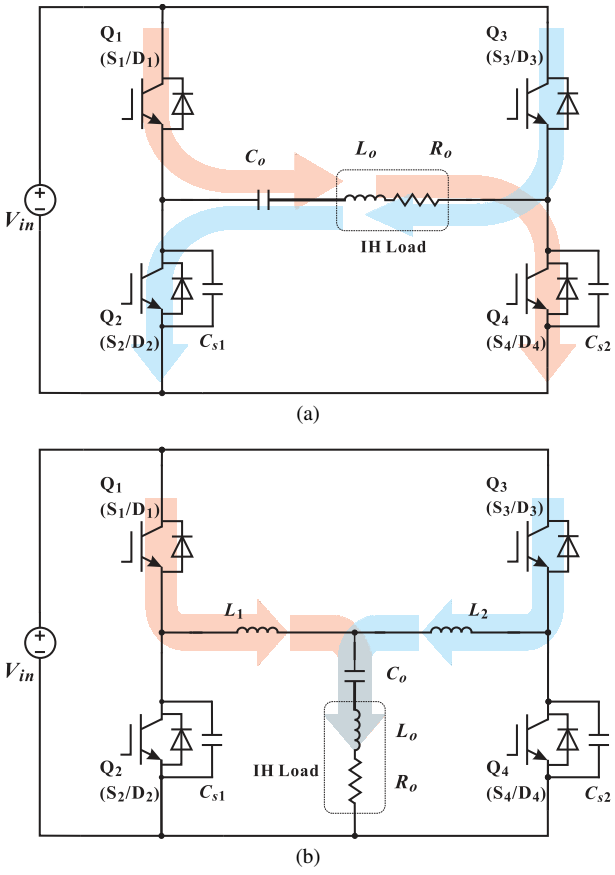

Fig. 3. Current pathway for IH load at full load (PS angle ϕ = 0 deg): (a) PS-PWM FB HF inverter, (b) proposed ZVS HF-R inverter.

The two inverters U_1 and U_2 produce the two resonant link currents i_{L1} and i_{L2} respectively, which are controlled by changing the PS angle ϕ in the IGBT gate pulse signals between Q_1-Q_2 and Q_3-Q_4 [17] [18]. Synthesizing the resonant link currents i_{L1} and i_{L2} yields the load current i_o with a lower harmonic distortion. Accordingly, the output power

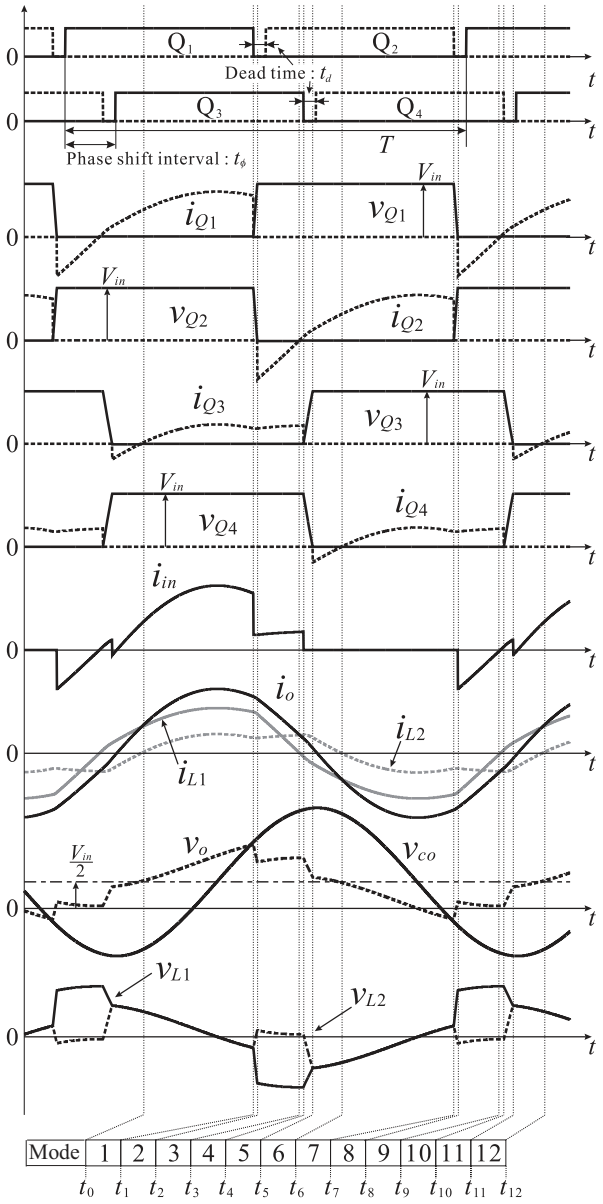

Fig. 4. Relevant voltage and current operating waveforms ($\phi = \omega t_\phi = 2\pi f_s t_\phi$).

injected into the IH working coil and load can be continuously controlled over the wide range of output power variations under the soft-switching condition. Since the IH load current is resulted by the two resonant link inductor currents, the HF inverter topology treated herein is suitable for increasing the power rating while reducing the conduction power losses, especially for the large and rated output power conditions.

The active switches Q_1-Q_2 and Q_3-Q_4 are commutated in ZVS due to the edge resonance by the lossless capacitors C_{s1} and C_{s2} with the aids of L_1 and L_2. The switching frequency f_s (= ω / 2π) of the two HF inverters can be designed and fixed to the value which is less than the inverter resonant frequency f_r defined by

$$f_r = \frac{1}{2\pi\sqrt{LC_o}}, \tag{1}$$

$$L = L_o + \frac{L_1 \cdot L_2}{L_1 + L_2}. \tag{2}$$

Since U_1 and U_2 are fundamentally designed to have the same power rating, L_2 is equal to L_1. Then, the inverter resonant switching frequency f_r is rewritten as

$$f_r = \frac{1}{2\pi\sqrt{LC_o}}, \tag{3}$$

$$L = L_o + \frac{L_r}{2}, \tag{4}$$

where $L_r = L_1 = L_2$.

As compared to the conventional ZVS PS-PWM FB HF inverter which is illustrated in Fig. 1, the proposed HF-R inverter has the advantages as

- The current rating of active switches can be reduced theoretically by half as compared to the ZVS PS-PWM FB HF inverter under the condition of same input dc voltage as illustrated in Fig. 3. Accordingly, the HF-R inverter proposed herein is effective for decreasing the conduction power losses in middle–heavy load power setting.
- No soft-switching limitation exists in the controlled-phase active switches, so minimization of switching power losses as well as the low EMI noise can be guaranteed for the wide-range output power variations.

B. Operation Principle

The operating waveforms of the proposed HF-R inverter are depicted in Fig. 4. The output power regulation is carried out by adjusting the PS angle ϕ (PS interval t_ϕ), which can be defined by

$$\phi = \frac{t_\phi}{T} \times 360 \ . \tag{5}$$

The switch-mode transitions and the resonant currents pathways in the proposed HF-R inverter are illustrated in Fig.5. The one switching cycle operation is divided into the twelve sub-modes as follows:

[Mode1 : $\mathbf{t_0 \le t < t_1}$] <*positive half-cycle steady-state power delivering mode*>: The resonant link currents i_{L1}, i_{L2} flow from the input dc power source V_{in} to the IH load through S_1 of Q_1 and S_3 in Q_3.

[Mode2 : $\mathbf{t_1 \le t < t_2}$] <Q_1 *ZVS turn-off mode*>: The gate signal to S_1 of Q_1 is removed at $t = t_1$. Then, the voltage v_{Q1} across Q_1 rises gradually by charging C_{s1}, while the voltage v_{Q2} across Q_2 declines with a certain slope from V_{in}. Thus, the ZVS turn-off operation begins in Q_1. During this interval, the inductive energy stored in the resonant link inductor L_1 should be greater than the capacitive energy of C_{s1} for completing ZVS operation due to the edge resonance in L_1 and C_{s1}. Thus, ZVS condition in Q_1 and Q_2 is defined by

$$\frac{1}{2}L_1 i_{L1}(t_1)^2 > \frac{1}{2}C_{s1}{V_{in}}^2. \tag{6}$$

Furthermore, the voltage v_{Q1} across Q_1 during its turn-on transition interval is expressed by

$$v_{Q1}(t) = Z_{q1} i_{L1}(t_1) \sin\omega_{q1}(t - t_1) \simeq Z_{q1} i_{L1}(t_1)(t - t_1) \tag{7}$$

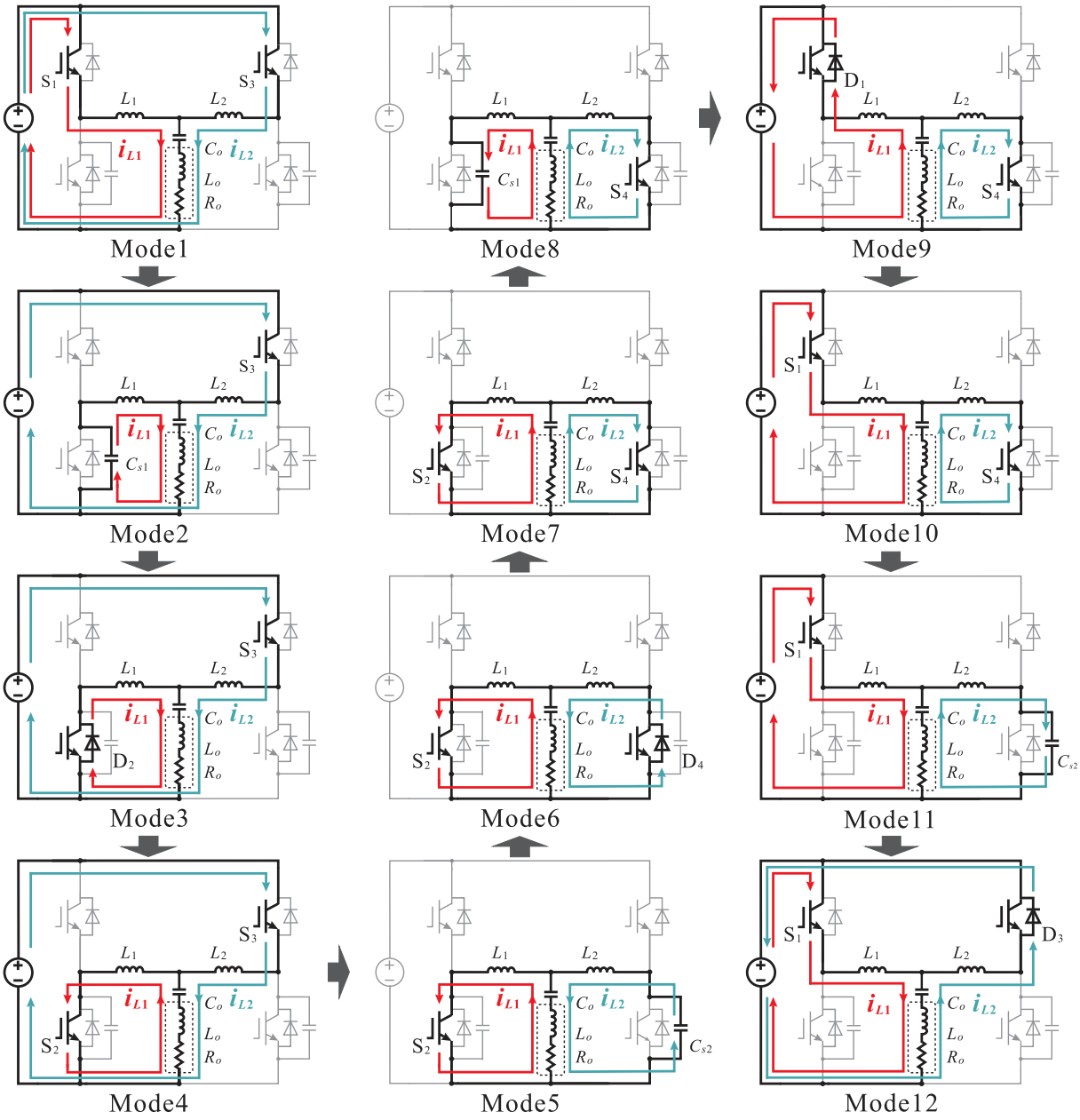

Fig. 5. Mode transitions during one switching cycle ($\phi = \omega t_\phi = 2\pi f_s t_\phi$).

where $Z_{q1} = \sqrt{L_1/C_{s1}}$ and $\omega_{q1} = 1/\sqrt{L_1 C_{s1}}$.

[Mode3 : $\mathbf{t_2 \le t < t_3}$] <Q_2 *Zero voltage and Zero Current Soft-Switching (ZVZCS) turn-on mode*>: The voltage v_{Q1} across Q_1 reaches V_{in} and the ZVS turn-off operation of Q_1 is competed at $t = t_2$, while the voltage v_{Q2} across Q_2 decreases to zero. Then, the anti-parallel diode D_2 in Q_2 is naturally forward-biased, thereby ZVZCS turn-on can be achieved in Q_2.

[Mode4 : $\mathbf{t_3 \le t < t_4}$] <U_1 *resonant link current reversely-circulating mode*>: The current through Q_2 commutates from D_2 to S_2 at $t = t_3$ owing to the series resonance in U_2. Accordingly, the resonant link current i_{L1} in U_1 circulates through L_1, S_2 and the IH load with C_o. In this transition, the current i_{L1} and i_{L2} have the reverse directions each other. This transition contributes for the output power regulation in the proposed HF-R inverter.

[Mode5 : $\mathbf{t_4 \le t < t_5}$] <Q_3 *ZVS turn-off mode*>: The gate signal to S_3 of Q_3 is removed at $t = t_4$. Then, the voltage v_{Q3} across Q_3 rises gradually by charging C_{s2}, while the voltage v_{Q4} across Q_4 declines with a gradient from V_{in}. Thus, ZVS turn-off operation begins in Q_3. During this interval, ZVS condition deriving from edge resonance by L_2 and C_{s2} is defined in a similar way to (6) as

$$\frac{1}{2} L_2 i_{L2}(t_4)^2 > \frac{1}{2} C_{s2} V_{in}{}^2. \tag{8}$$

Furthermore, the voltage v_{Q3} across Q_3 during its turn-off transition interval is expressed by

$$v_{Q3}(t) = Z_{q2} i_{L2}(t_4) \sin \omega_{q2}(t - t_4) \simeq Z_{q2} i_{L2}(t_4)(t - t_4), \tag{9}$$

where $Z_{q2} = \sqrt{L_2/C_{s2}}$ and $\omega_{q2} = 1/\sqrt{L_2 C_{s2}}$.

[Mode6 : $\mathbf{t_5 \le t < t_6}$] <Q_4 *ZVZCS turn-on mode*>: The voltage

v_{Q3} across Q_3 reaches V_{in} at $t = t_5$ and the ZVS turn-off operation of Q_3 is completed, while the voltage v_{Q4} across Q_4 decreases down to zero. Then, the anti-parallel diode D_4 in Q_4 is naturally forward-biased, thereby ZVZCS turn-on can be achieved in Q_4.

[Mode7 : $t_6 \le t < t_7$] <*negative half-cycle steady-state power delivering mode*>: The resonant link current i_{L2} in U_2 naturally commutates from D_4 to S_4 at $t = t_6$. Then, the two resonant link currents i_{L1}, i_{L2} flow through the IH load in the same direction.

[Mode8 : $t_7 \le t < t_8$] <Q_2 *ZVS turn-off mode*>: The gate signal to S_2 of Q_2 is removed at $t = t_7$. Then, the voltage v_{Q2} across Q_2 rises gradually by charging C_{s1}, while the voltage v_{Q1} across Q_1 declines with a certain slope from V_{in}. Thus, ZVS turn-off operation begins in Q_2. During this interval, ZVS condition due to the edge resonance in L_1 and C_{s1} is defined by

$$\frac{1}{2}L_1 i_{L1}(t_7)^2 > \frac{1}{2}C_{s1}{V_{in}}^2. \tag{10}$$

Furthermore, the voltage v_{Q2} across Q_2 during its turn-off transition interval is expressed by

$$v_{Q2}(t) = Z_{q1} i_{L1}(t_7) \sin \omega_{q1}(t - t_7) \simeq Z_{q1} i_{L1}(t_7)(t - t_7). \tag{11}$$

[Mode9 : $t_8 \le t < t_9$] <Q_1 *ZVZCS turn-on mode*>: The voltage v_{Q2} across Q_2 reaches V_{in} at $t = t_8$ and the ZVS turn-off operation is completed in Q_2, while the voltage v_{Q1} across Q_1 decreases to zero. Then, the anti-parallel diode D_1 in Q_1 is naturally forward-biased, thereby ZVZCS turn-on can be achieved in Q_1. During this interval, a part of the IH load current is fed back to the input dc voltage source V_{in} via the resonant link inductor L_1.

[Mode10 : $t_9 \le t < t_{10}$] <U_2 *resonant link current reversely-circulating mode*>: The current through Q_1 commutates from D_1 to S_1 at $t = t_9$ owing to the series resonance in U_1. Then, the power begins to be delivered to the IH load through the resonant link inductor L_1, while the resonant link current i_{L2} in U_2 circulates through L_2, S_4 and the IH load with C_o. In this transition, the resonant link currents i_{L1} and i_{L2} have the reverse directions each other. This transition contributes for the output power regulation as well as Mode 4.

[Mode11: $t_{10} \le t < t_{11}$] <Q_4 *ZVS turn-off mode*>: The gate signal to S_4 of Q_4 is removed at $t = t_{10}$. Then, the voltage v_{Q4} across Q_4 rises gradually by charging C_{s2}, while the voltage v_{Q3} across Q_3 declines slowly from V_{in}. Thus, ZVS turn-off begins in Q_4. During this interval, ZVS condition due to the edge resonance by L_2 and C_{s2} is defined by

$$\frac{1}{2}L_2 i_{L2}(t_{10})^2 > \frac{1}{2}C_{s2}{V_{in}}^2. \tag{12}$$

Furthermore, the voltage v_{Q4} across Q_4 during its turn-off transition interval is expressed by

$$v_{Q4}(t) = Z_{q2} i_{L2}(t_{10}) \sin \omega_{q2}(t - t_{10}) \simeq Z_{q2} i_{L2}(t_{10})(t - t_{10}). \tag{13}$$

[Mode12 : $t_{11} \le t < t_{12}$] <Q_3 *ZVZCS turn-on mode*>: The voltage v_{Q4} across Q_4 reaches V_{in} at $t = t_{11}$ and the ZVS turn-off operation is completed in Q_4, while the voltage v_{Q3} across Q_3 decreases to zero. Then, the anti-parallel diode D_3 in Q_3 is naturally forward-biased, thereby ZVZCS turn-on can be achieved in Q_3.

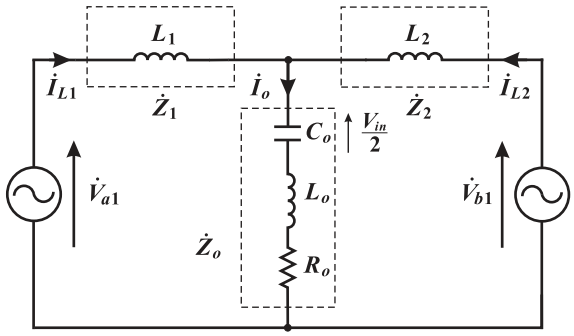

Fig. 6. Frequency-domain equivalent circuit based on two dc-biased fundamental frequency ac voltage sources.

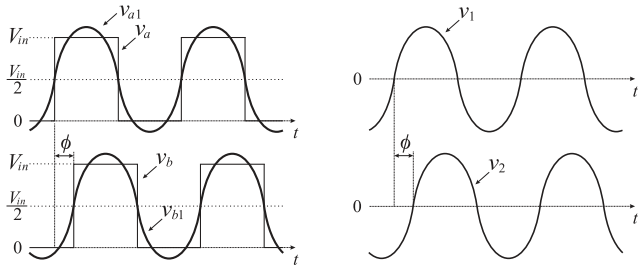

(a) (b)

Fig. 7. Rectangular waveform voltage across middle point (a, b) of each inverter leg and negative dc bus line: (a) dc-biased, (b) non-dc biased.

III. Analysis of Output Power Regulation Based on Equivalent Circuit

The frequency-domain equivalent circuit of the proposed HF-R inverter is illustrated in Fig. 6. The complex voltage vectors $\dot{V}_{a1}$ and $\dot{V}_{b1}$ represent the fundamental components of the $V_{in}/2$ dc biased rectangular waveforms v_a and v_b as depicted in Fig. 7 (a), which appear between the middle points a, b and the negative dc busline on the asymmetrical half-bridge inverter units U_1 and U_2, respectively. For simplifying the analysis of power regulation principle in the proposed HF-R inverter, the non-dc-biased rectangular waveforms v_1 and v_2 are introduced as depicted in Fig. 7 (b).

The root mean square (RMS) value V of the fundamental components v_{a1} and v_{b1} can be defined by Fourier Series Expansion as

$$V = \frac{\sqrt{2}V_{in}}{\pi}. \tag{14}$$

Accordingly, $\dot{V}_1$ and $\dot{V}_2$ can be expressed with the PS angle ϕ as

$$\dot{V}_1 = V, \tag{15}$$

$$\dot{V}_2 = V\, e^{-j\phi}. \tag{16}$$

In Fig. 8, the two kinds of equivalent circuits, i.e., Superposition Principle model and Thevenin's Theorem model can be derived from Fig. 6. Based on the Superposition model in Fig. 8 (a), the two resonant link currents phasors $\dot{I}_{L1}$, $\dot{I}_{L2}$ and the IH load current phasor $\dot{I}_o$ $(= \dot{I}_{L1} + \dot{I}_{L2}\angle\theta,\ \theta = \angle\dot{I}_{L1} - \angle\dot{I}_{L2})$ can be defined as

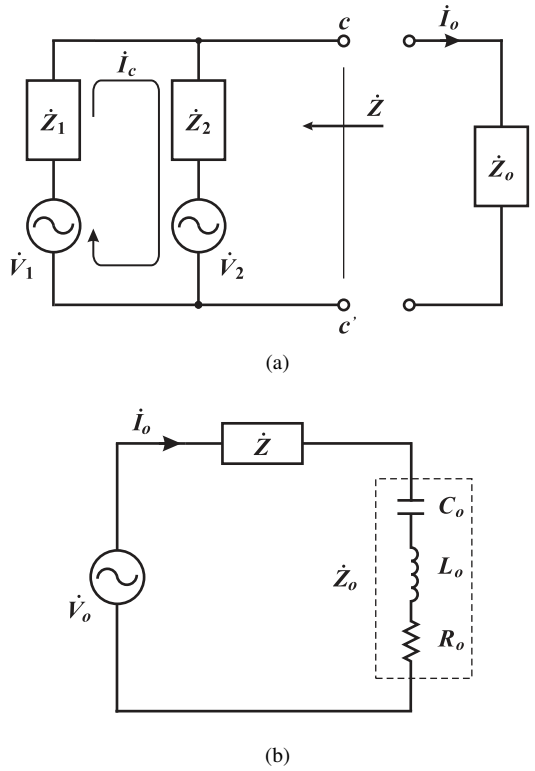

Fig. 8. Equivalent circuits with non-dc biased ac voltage sources: (a) superposition principle, (b) Thevenin's theorem.

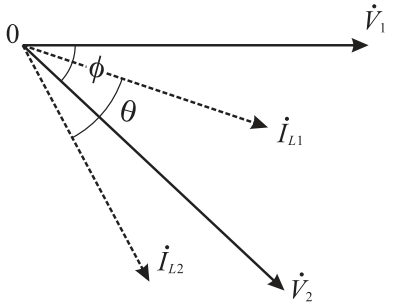

Fig. 9. Two half-bridge inverter units U_1, U_2 voltage and current phasors.

$$\dot{I}_{L1} = \frac{V\left\{1 + \frac{\dot{Z}_o}{\dot{Z}_1}A(1 - e^{-j\phi})\right\}}{2\dot{\Gamma}}, \tag{17}$$

$$\dot{I}_{L2} = \frac{VA\left\{e^{-j\phi} - \frac{\dot{Z}_o}{\dot{Z}_1}(1 - e^{-j\phi})\right\}}{2\dot{\Gamma}}, \tag{18}$$

$$\dot{I}_o = \frac{V(1 + Ae^{-j\phi})}{2\dot{\Gamma}}, \tag{19}$$

$$A = \frac{\dot{Z}_1}{\dot{Z}_2} = \frac{L_1}{L_2}, \tag{20}$$

$$\dot{\Gamma} = \left(\frac{1+A}{2}\right)\dot{Z}_o + \frac{\dot{Z}_1}{2} = R_o\left\{\left(\frac{1+A}{2}\right) + jQ\left(\frac{\omega}{\omega_r} - \frac{\omega_r}{\omega}\right)\right\} \tag{21}$$

$$\omega = \frac{2\pi}{T}, \quad \omega_r = \frac{1}{\sqrt{LC_o}}, \tag{22}$$

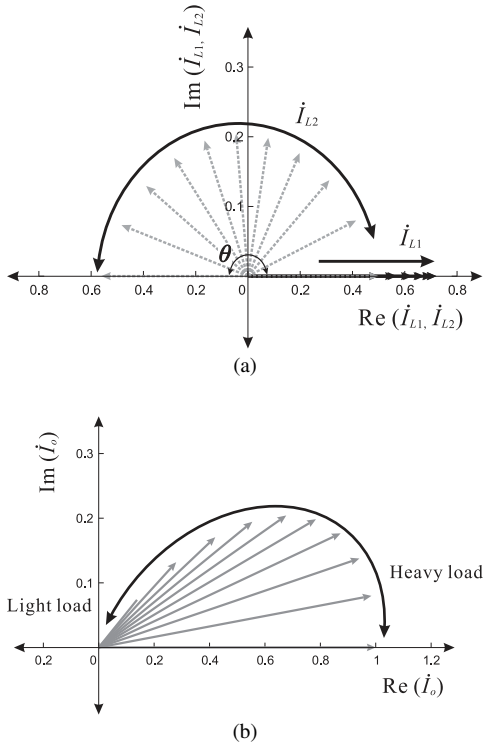

Fig. 10. Phasor diagrams of resonant link inductors and IH load current: (a) resonant link currents, (b) IH load current.

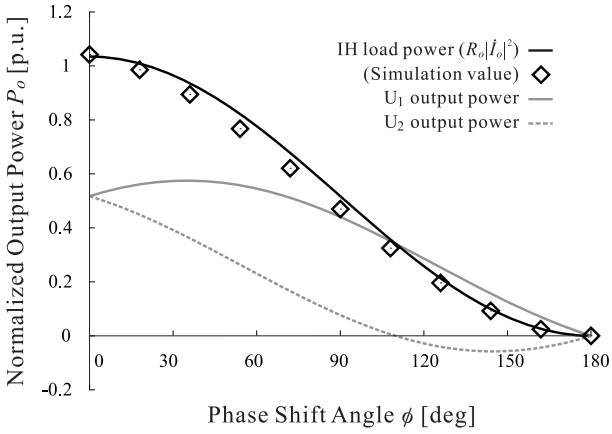

Fig. 11. Relationship between output power and phase-shift angle.

$$Q = \frac{\omega_r\left\{(1+A)L_o + L_1\right\}}{2R_o} = \frac{1+A}{2\omega_r C_o R_o}, \tag{23}$$

where Q denotes the loaded quality factor and A represents the resonant link inductors ratio, respectively. Accordingly, the IH load power can be determined by

$$P_o = R_o|\dot{I}_o|^2. \tag{24}$$

The phase angle relationship between the complex voltage vector $\dot{V}_1, \dot{V}_2$ and current vectors $\dot{I}_{L1}, \dot{I}_{L2}$ is illustrated in Fig. 9. It should be noted here that the phase difference angle θ between $\dot{I}_{L1}$ and $\dot{I}_{L2}$ is equal to ϕ when L_1 and L_2 are the same inductance. Based on (17)–(23), the phasor diagrams of the PS-controlled resonant link currents and the resultant IH load current are indicated in Fig. 10. It can be known herein

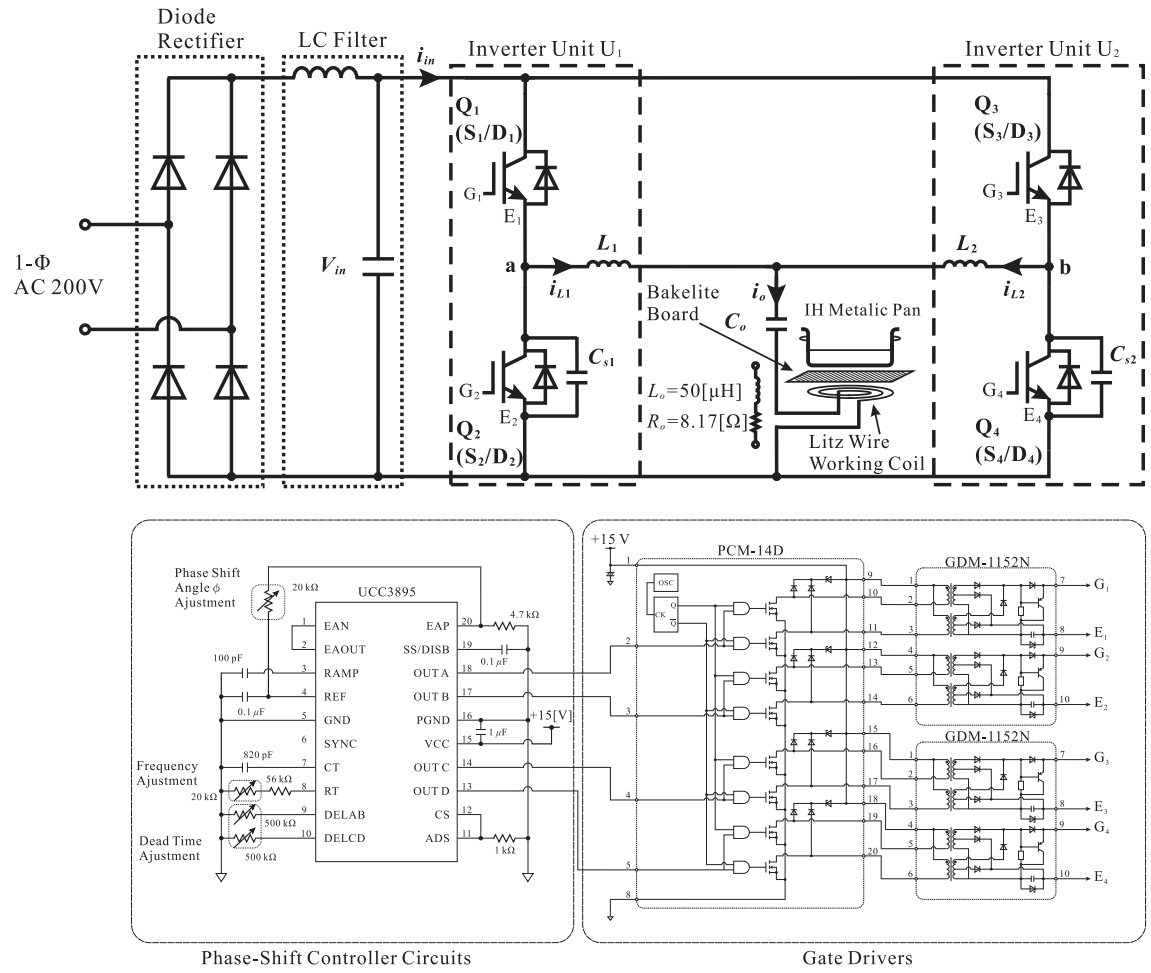

Fig. 12. Schematic diagram of the experimental main circuit and gate pulse generator with gate drivers (in open loop control).

that the load current phasor $\dot{I}_o$ can be continuously controlled by varying the PS angle ϕ.

The cross current $\dot{I}_c$ between U_1 and U_2 as depicted in Fig. 8 (a), which is outstanding in the low output power settings can be expressed in RMS by

$$I_c = \left| \frac{\dot{V}_1 - \dot{V}_2}{\dot{Z}_1 + \dot{Z}_2} \right| = \frac{2V}{\omega(L_1 + L_2)} \tag{25}$$

The another equivalent circuit, Thevenin's Theorem model, is shown in Fig. 8 (b). In this equivalent circuit, the two ac voltages sources $\dot{V}_1$ and $\dot{V}_2$ can be expressed by just one ac voltage source (Thevenin's equivalent voltage source) $\dot{V}_o$ as

$$\dot{V}_o = \frac{(1 + e^{-j\phi})\dot{V}}{2}. \tag{26}$$

In addition, the two resonant link inductors L_1 and L_2 can be simply expressed by one internal impedance $\dot{Z}$ as

$$\dot{Z} = \frac{\dot{Z}_1 \dot{Z}_2}{\dot{Z}_1 + \dot{Z}_2} = j\omega \left(\frac{L_1 L_2}{L_1 + L_2} \right). \tag{27}$$

Thus, the Thevenin's Theorem model is useful for facilitating the analysis of power regulation in the proposed HF-R inverter.

Theoretical curves of active powers in the two inverters U_1, U_2 and the IH load vs. PS angle characteristics are depicted in Fig. 11, where the relevant simulation values are plotted for showing the accuracy of the theoretical equations through (14) to (24). It can be understood from Fig. 11 that the IH load power as well as output power of each inverter unit can be continuously controlled by varying the PS angle ϕ, which facilitates the seamless output power regulation in the proposed HF-R inverter.

IV. Experimental Results and Evaluations

A. Design Procedure for Laboratory Prototype

Performances of the soft switching operation and the output power regulation based on the current phasor control are evaluated in an experiment with the small-scale 1 kW-60 kHz laboratory prototype.

The schematic diagram of the experimental set-up with an open loop controller is illustrated in Fig. 12. The open loop method is employed for the prototype in order to focus on investigating the validity of the proposed HR-R inverter circuit topology in the experiment. The gate pulse signals for the active switches Q_1–Q_4 are generated by a PS-PWM controller *UCC3895* (Texas Instruments) as depicted in Fig. 12. The exterior appearance of the experimental set-up is portrayed in Fig. 13. In this experiment, the actual efficiency

TABLE I
DESIGN SPECIFICATIONS AND CIRCUIT PARAMETERS OF PROTOTYPE.

Parameter		Value [unit]
Output power rating P_o		1 kW
DC input voltage V_{in}		240 V
Resonant inductor L_1,L_2		44 μH
Power factor tuned capacitor C_o		0.112 μF
Lossless snubbing capacitors C_{s1},C_{s2}		6 nF
IH load (Iron pan)	Equivalent effective resistance R_o	8.17 Ω
	Equivalent effective inductance L_o	50 μH
Switching frequency f_s		60 kHz
Inverter resonant frequency f_r		56 kHz
Dead time t_d		0.5 μs
Q_1–Q_4: IXGN60N60C2D1 600 V, 75 A		
Phase shift PWM IC:UCC3895		
Gate driver: GDM-1152N		

$\eta\,(=P_o/P_{in})$ is measured for the dc–HF ac power conversion stage by using a precision power analyzer YOKOGAWA *WT 1800* ($\pm\{(0.3\times f_s - 9.5)\,\%$ of reading + 1 % of range$\}$) as drawn in Fig. 14. In order to focus on evaluations of the essential performances in the proposed HF-R inverter and simplify the experimental set-up configuration, the iron pan is employed here in stead of aluminum and copper pans which would demand an additional impedance matching transformer.

The design specifications of the proposed HF-R inverter and experimental conditions are listed in TABLE I. The equivalent effective resistance R_o and inductance L_o of the IH load can be estimated from the transformer representation of the electromagnetic induction between the IH working coil and the metallic pan[19]. By setting the switching frequency f_s = 60 kHz, the PFC tuned capacitor C_o can be calculated with L_o as

$$C_o = \frac{1}{\omega^2 L_o} = \frac{1}{(2\pi f_s)^2 L_o} = 0.112\,\mu\text{F}. \qquad (28)$$

The loaded quality factor Q = 3.0 is given herein so that the voltage across C_o does not exceed its rated value 800 Vrms. Accordingly, the inverter resonant frequency f_r can be set to be 56 kHz from (3) for assuring the inductive load conditions and ZVS operations in Q_1–Q_4.

In this experimental evaluation, it is assumed that the inverter units U_1 and U_2 have the symmetric circuit parameters and the same power rating. Accordingly, the resonant link inductors $L_r = L_1 = L_2$ can be designed from (3) as

$$L_r = 2\left(\frac{1}{\omega_r^2 C_o} - 1\right) = 2\left\{\frac{1}{(2\pi f_r)^2 C_o} - 1\right\} = 44\,\mu\text{H}. \qquad (29)$$

B. Inverter Operating Waveforms

The resonant link currents i_{L1}, i_{L2}, IH load current i_o, the HF-R inverter output voltage v_o and the PFC turned capacitor voltage v_{co} for the full and no load conditions are illustrated in Fig. 15 for simulation results obtained by PSIM Ver.9-2, and in Fig. 16 for the corresponding measured waveforms, respectively. The amplitudes of the fixed and controlled-phase currents i_{L1}, i_{L2} are continuously regulated in accordance with the PS angle ϕ as illustrated in Fig. 10. It can also be confirmed

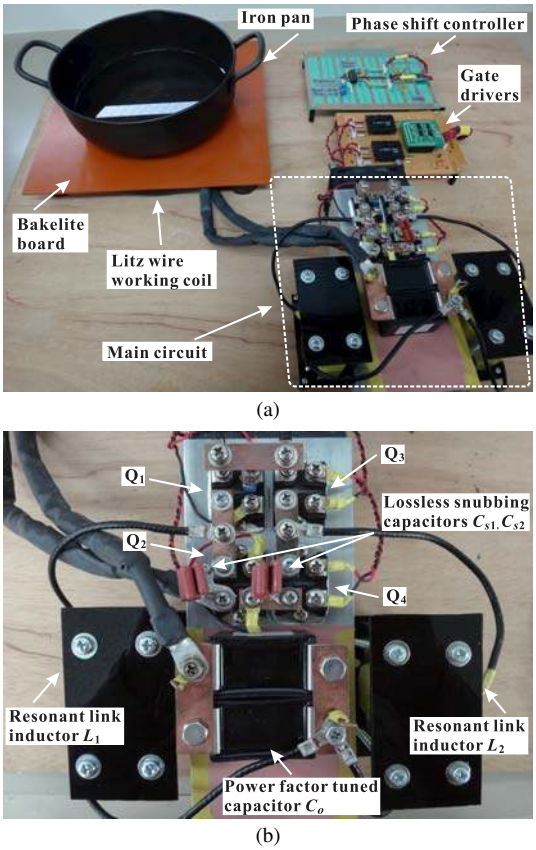

Fig. 13. Exterior appearance of the proposed HF-R inverter prototype: (a) experimental set-up, (b) main circuit.

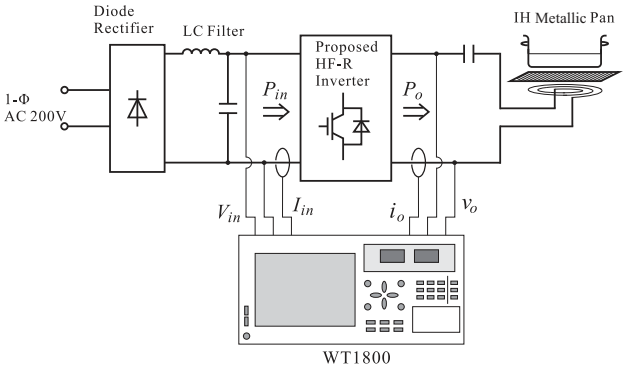

Fig. 14. Measurement set-up of actual efficiency in HF inverter prototype.

from the measured waveforms of i_o, v_o and v_{co} that more power is supplied into the IH load as the PS angle command gets smaller. The good agreement can be confirmed between the simulation and experimental waveforms of the steady-state operating waveforms in the proposed HF-R inverter.

The switching performances of Q_1 & Q_2 in the fixed-phase inverter U_1 and Q_3 & Q_4 in the controlled-phase inverter U_2 are depicted in Figs. 17 and 18, respectively. In addition, the enlarged waveforms of the fixed-phase and controlled phase switches are depicted for the rated output power condition in Fig. 19, and for the null load condition in Fig. 20. Furthermore, the voltage and current Lissajous figures of Q_1 and Q_3 are

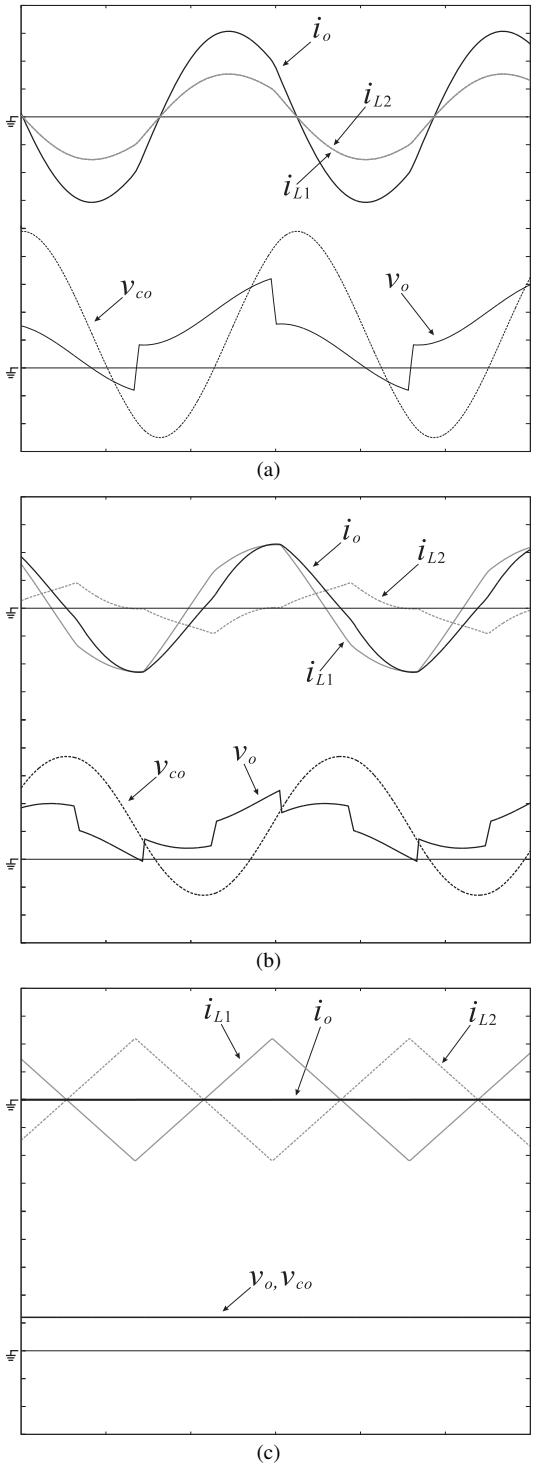

Fig. 15. Simulated steady-state operating waveforms: (a) P_o = 1 kW, ϕ = 0 deg, (b) P_o = 400 W, ϕ = 90 deg, (c) P_o = 0 W, ϕ = 180 deg (100 V/div, 5A/div, 5μs/div).

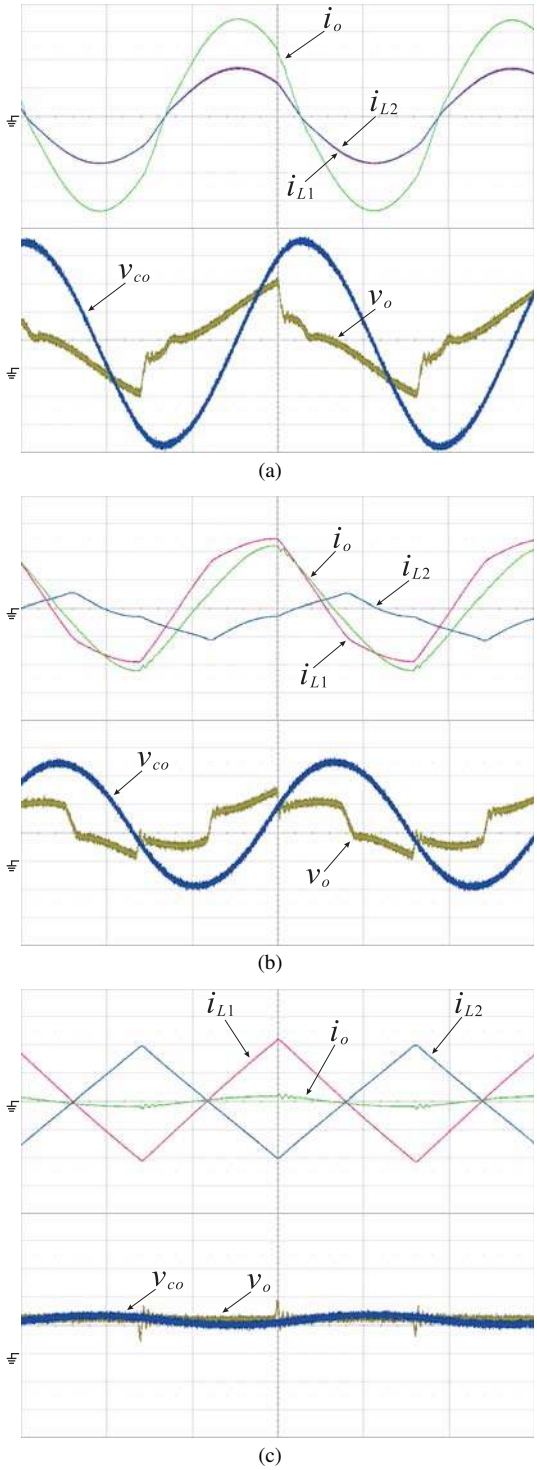

Fig. 16. Experimental steady-state operating waveforms: (a) P_o = 1 kW, ϕ = 0 deg, (b) P_o = 400 W, ϕ = 90 deg, (c) P_o = 0 W, ϕ = 180 deg (100 V/div, 5 A/div, 5μs/div).

indicated for the large output setting in Fig. 21 and for the no load setting in Fig. 22, respectively. It can be confirmed that ZVS operations are achievable and maintain in all the active switches regardless of the load power settings. ZVZCS turn-on and ZVS turn-off operations are achievable even for the null load condition, thereby the wide-range (100 % – 0 % load) soft-switching performances are actually demonstrated. Thus, it can be expected that EMI noise can be reduced over the wide load range in the proposed HF-R inverter.

The switching waveforms of the fixed-phase active switches Q_1 & Q_2 and the controlled-phase active switches Q_3 & Q_4 in the ZVS PS-PWM FB HF inverter under the same conditions of power rating, input dc voltage, switching frequency and IH load parameters as the proposed HF-R inverter prototype

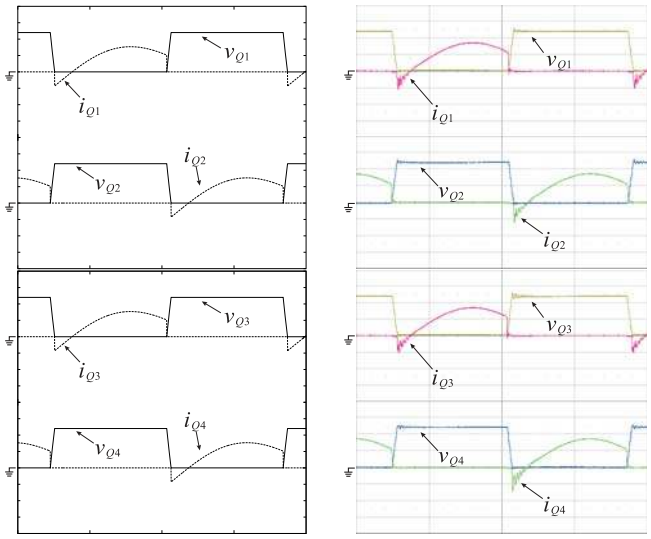

Fig. 17. Switching waveforms in the proposed HF-R inverter at P_o = 1 kW, ϕ = 0 deg: (a) simulated waveforms, (b) experimental waveforms (100V/div, 5A/div, 5μs/div).

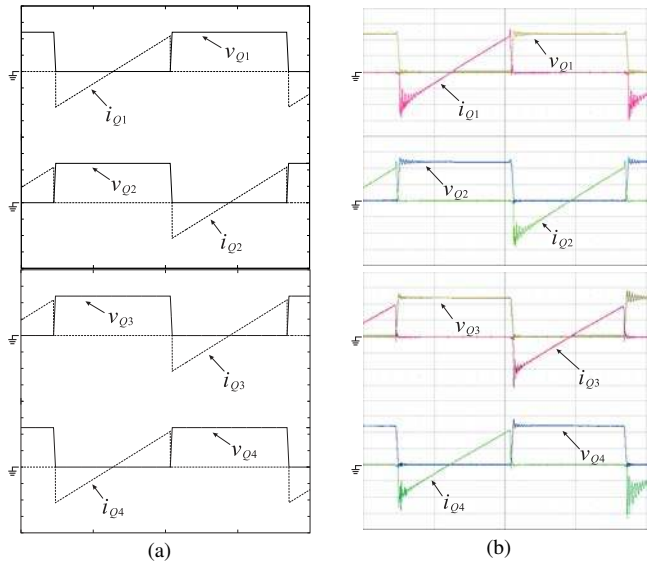

Fig. 18. Switching waveforms in the proposed HF-R inverter at P_o = 0 W, ϕ = 180 deg: (a) simulated waveforms, (b) experimental waveforms (100 V/div, 5 A/div, 5 μs/div).

are drawn in Fig. 23. In addition, the enlarged waveforms of the fixed-phase and controlled-phase switches are depicted for the rated output power condition in Fig. 24, and for almost the null load condition in Fig. 25. The corresponding voltage and current Lissajous figures of the fixed-phase switch Q_1 and the controlled-phase switch Q_3 are portrayed for the rated output power condition in Fig. 26 and for the low output power condition in Fig. 27, respectively. It is clearly demonstrated in Fig. 23 (d), Fig. 25 (b) and Fig. 26 (d) that the complete ZVS operations are lost in the controlled-phase active switches in the low output power setting because the residual voltage exists in the lossless snubbing capacitor C_{s2}. As a result, the soft-switching range is limited in 100 % – 20 % load setting area.

It can be observed in Fig. 17 (b) and Fig. 23 (a),(b) that the peak current of the active switches are actually reduced by half in the proposed HF-R inverter as compared to the ZVS PS-PWM FB HF inverter. Actually, the RMS current of active switches in the proposed HF-R inverter is 4.25 A, while 8.45 A is measured in the ZVS PS-PWM FB HF inverter. Thus, it is actually proven that the smaller current rating power devices can be employed for the proposed HF-R inverter.

C. Power Regulation Characteristics

The measured output power P_o vs. PS angle ϕ curves are depicted in Fig. 28. The experimental characteristics demonstrated herein can well agree with those of the theoretical and simulation analysis in Fig. 11. It is actually proven herein that the wide-range output power regulation can be attained by the current phasor control.

The actual power conversion efficiencies of the proposed HF-R inverter and ZVS PS-PWM FB HF inverter are compared in Fig. 29. The proposed HF-R inverter attains the higher efficiency in the power range of 0.4 kW–1 kW (40 %–100 % load settings). This is essentially due to the lower

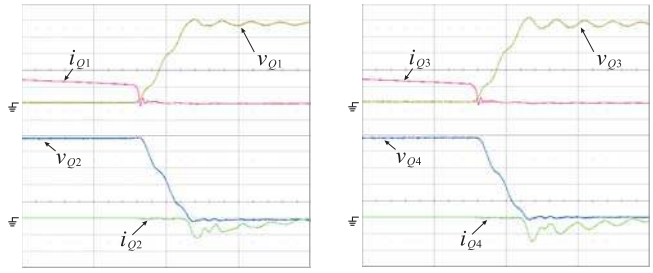

Fig. 19. Enlarged switching waveforms in the proposed HF-R inverter at P_o = 1 kW: (a) fixed-phase switches Q_1&Q_2, (b) controlled-phase switches Q_3&Q_4 (50 V/div, 5A/div, 500 ns/div).

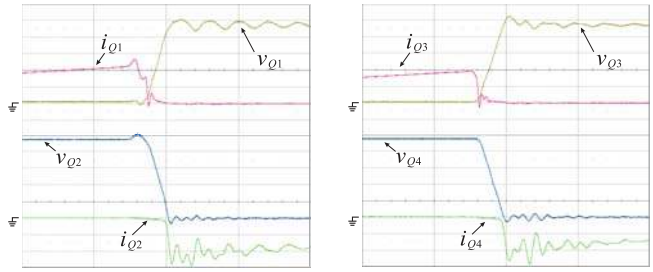

Fig. 20. Enlarged switching waveforms in the proposed HF-R inverter at P_o = 0 W: (a) fixed-phase switches Q_1&Q_2, (b) controlled-phase switches Q_3&Q_4 (50 V/div, 5A/div, 500 ns/div).

conduction power losses of the active switches in the proposed HF-R inverter. The maximum efficiency 96.3 % is obtained at P_o = 1 kW. In the case of implementing the PS angle control only, the conversion efficiency declines gradually and lowers than 90 % in the power range below P_o = 400 W with ϕ = 90 deg. This is due to occurrence of the relatively large peak currents which circulate through the resonant link inductors for the low output power settings as indicated in Fig. 16 (c) and Fig. 18 (b). Those cross currents cause the

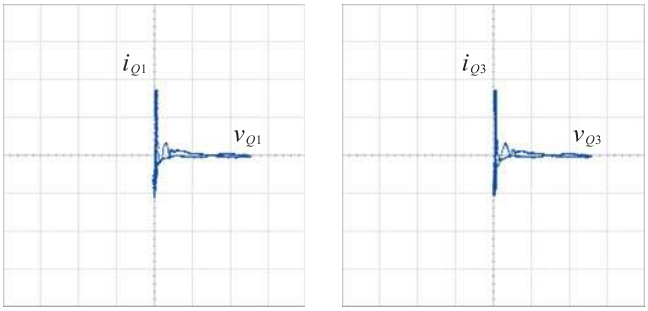

Fig. 21. Experimental current-voltage traces for switching transitions in proposed HF-R inverter at P_o = 1 kW, ϕ = 0 deg: (a) fixed-phase Q_1, (b) controlled-phase Q_3 (100 V/div, 5 A/div).

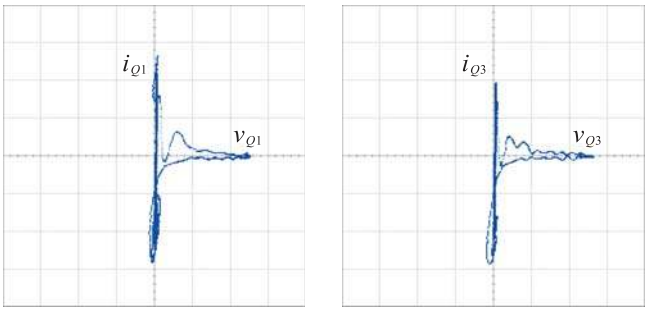

Fig. 22. Experimental current-voltage traces for switching transitions in proposed HF-R inverter at P_o = 0 W, ϕ = 180 deg: (a) fixed-phase Q_1, (b) controlled-phase Q_3 (100V/div, 5A/div).

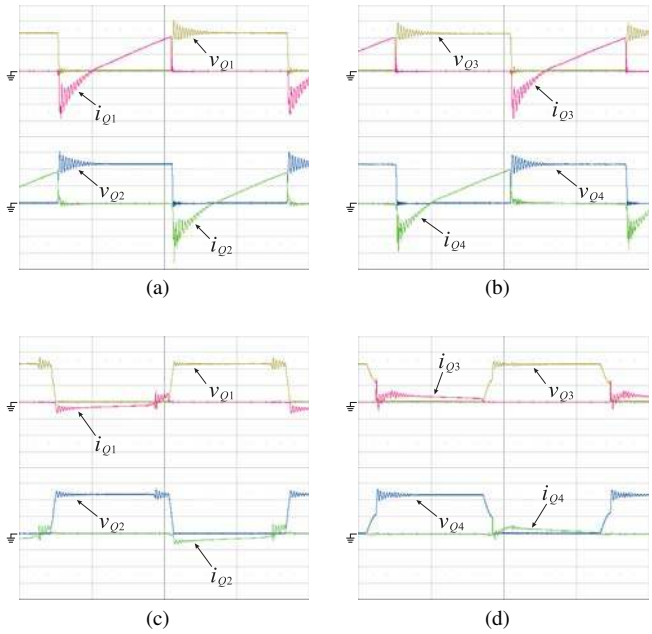

Fig. 23. Switching waveforms of ZVS PS-PWM FB HF inverter: (a) fixed-phase Q_1&Q_2 (P_o = 1 kW, ϕ = 0 deg), (b) controlled-phase Q_3&Q_4 (P_o = 1 kW, ϕ = 0 deg), (c) fixed-phase Q_1&Q_2 (P_o = 60 W, ϕ = 144 deg), (d) controlled-phase Q_3&Q_4 (P_o = 60 W, ϕ = 144 deg) (100V/div, 10A/div, 5μs/div).

efficiency deterioration for the low output power conditions while they work effectively for attaining ZVS commutations in $Q_1 - Q_4$.

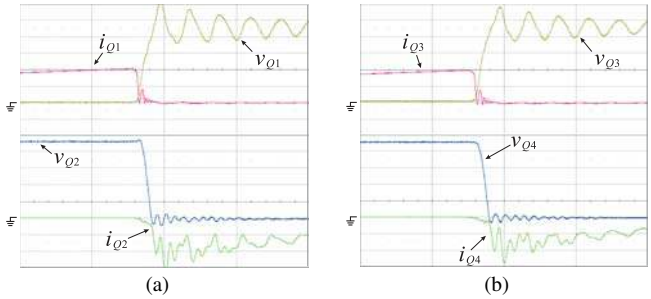

Fig. 24. Enlarged switching waveforms in the ZVS PS-PWM FB HF inverter at P_o = 1 kW: (a) fixed-phase switches Q_1&Q_2, (b) controlled-phase switches Q_3&Q_4 (50 V/div, 10A/div, 500 ns/div).

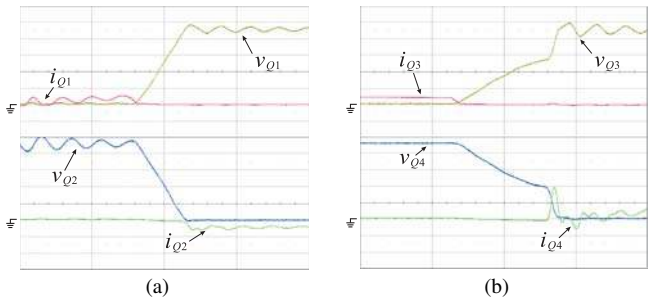

Fig. 25. Enlarged switching waveforms in the ZVS PS-PWM FB HF inverter at P_o = 0 W: (a) fixed-phase switches Q_1&Q_2, (b) controlled-phase switches Q_3&Q_4 (50 V/div, 10A/div, 500 ns/div).

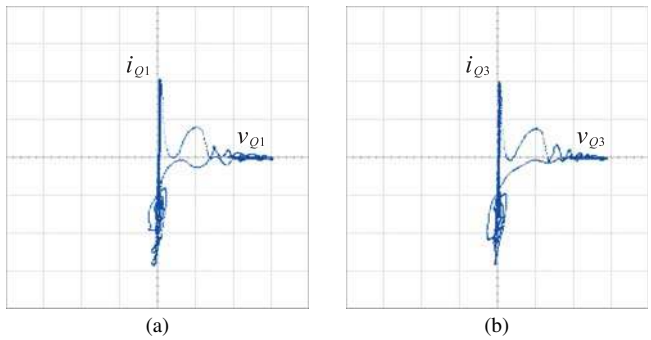

Fig. 26. Experimental current-voltage traces for switching transitions in ZVS PS-PWM FB HF inverter at P_o = 1 kW, ϕ = 0 deg: (a) fixed-phase Q_1, (b) controlled-phase Q_3 (100V/div, 10A/div).

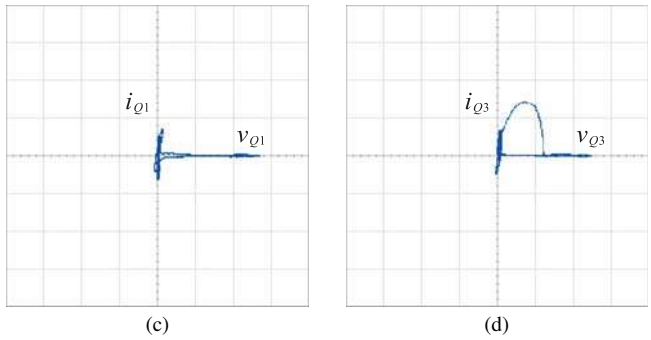

Fig. 27. Experimental current-voltage traces for switching transitions in ZVS PS-PWM FB HF inverter at P_o = 60 W, ϕ = 144 deg: (a) fixed-phase Q_1, (b) controlled-phase Q_3 (100V/div, 10A/div).

Fig. 30 shows that the state phase planes of the resonant

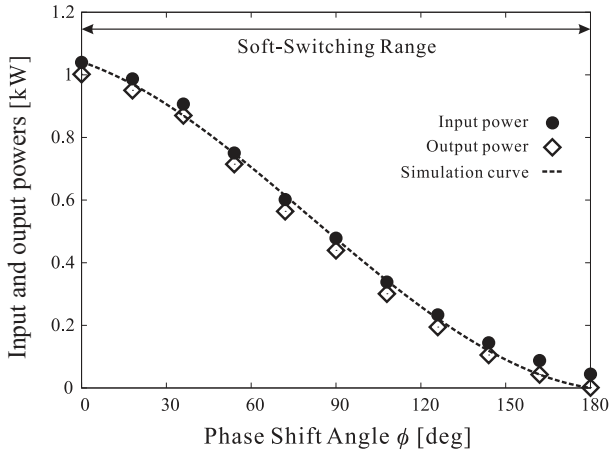

Fig. 28. Experimental characteristics of input and output powers vs. phase-shift angle.

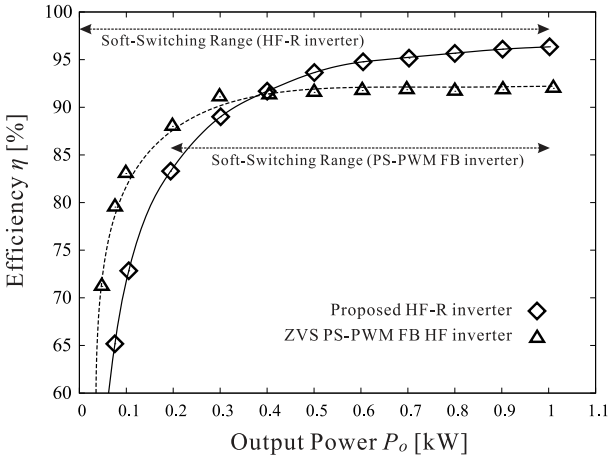

Fig. 29. Comparison of actual efficiencies vs. output power curves.

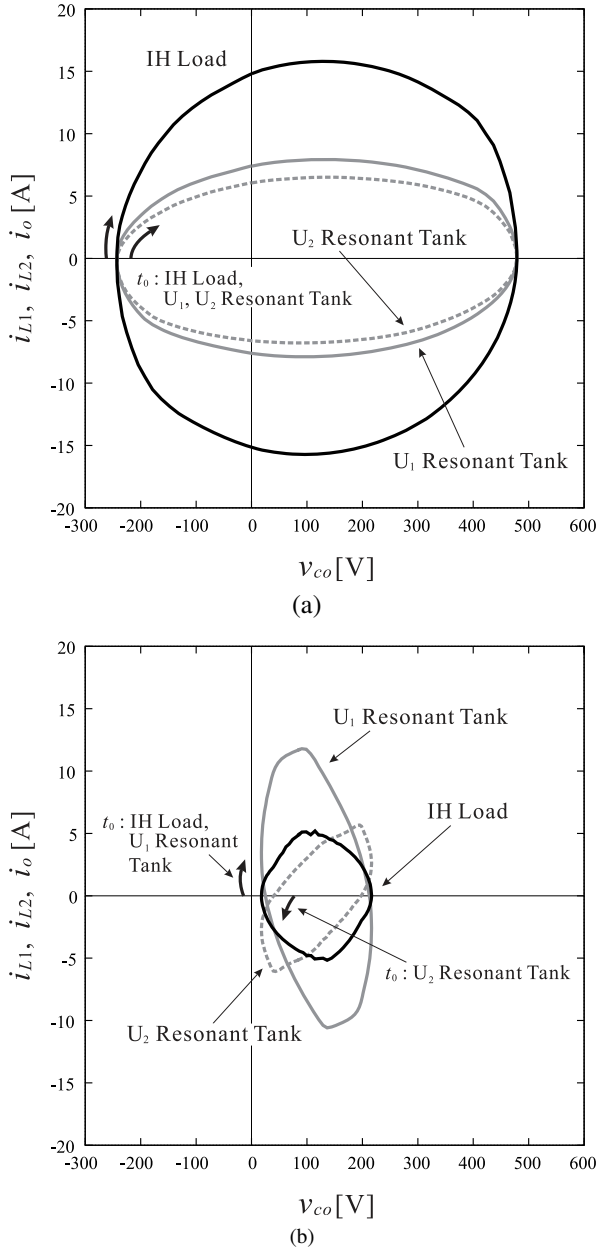

Fig. 30. Experimental state phase planes: (a) P_o = 1 kW, ϕ = 0 deg, (b) P_o = 100 W, ϕ = 145 deg.

voltages and currents in the IH load, the fixed-phased inverter unit U_1 and controlled-phase inverter unit U_2 under the load conditions of 100 % and 10 %, respectively. It can be observed therein that the resonant tank-stored energy in U_1 swells out in accordance with the decrease of IH load power, while that of U_1 shrinks gradually in the area of $0 < \phi < 90$ deg and expands out in the area of $90 < \phi < 180$ deg, respectively.

D. Efficiency Improvements for Light Loads

As one of the strategies for improving the efficiency under the condition of low output power, only the single inverter unit operates in the proposed HF-R inverter by the asymmetrical PWM scheme. It is obvious that the cross currents inherent to the two-inverter unit configuration can be eliminated completely in the single inverter. The gate pulse pattern of the asymmetrical PWM is illustrated in Fig. 31, where the duty cycle D is defined by

$$D = \frac{t_{on1}}{T}. \tag{30}$$

The simulated and experimental operating waveforms of the active switches and IH load with the asymmetrical PWM are depicted in Fig. 32. The enlarged switching voltage and current waveforms are also provided in Fig. 33, where ZVS operations can be observed in Q_1 and Q_2. The output power vs. duty cycle characteristics with the asymmetrical PWM are shown in Fig. 34. It can be observed that the proposed HF-R inverter operates from the middle to low output power area (from 50 % to 10 %) by the asymmetrical PWM scheme.

The actual efficiencies of the proposed HF-R inverter with the PS angle control and asymmetrical PWM are compared with that of the ZVS PS-PWM FB HR inverter in Fig. 35 for the output power range less than 400 W. It can be confirmed that 90 % can be achieved at P_o = 100 % by asymmetrical PWM while 73 % is measured by the PS angle control at the same output power, although the soft switching range decreases. Thus, the effectiveness of the asymmetrical PWM-

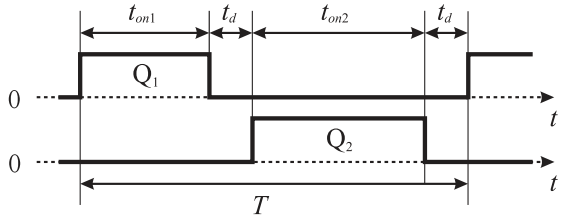

Fig. 31. Asymmetrical PWM pulse timing sequence.

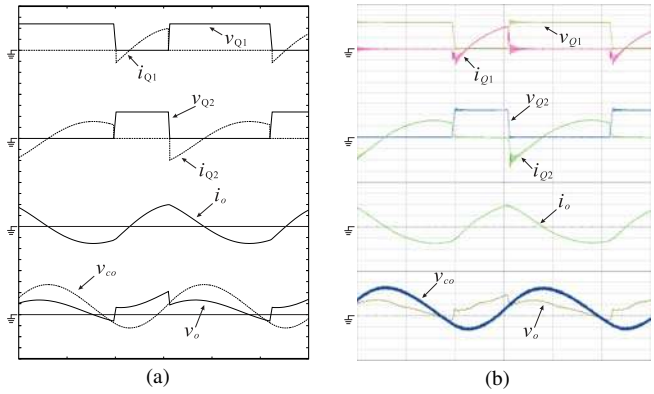

Fig. 32. Switching operations and IH load current waveforms under the condition of P_o = 300 W, D= 0.32 (100V/div, 5A/div, 5μs/div): (a) simulated waveforms, (b) experimental waveforms.

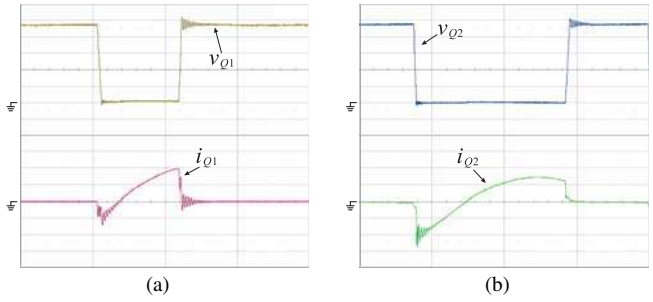

Fig. 33. Enlarged switching waveforms in the asymmetrical-PWM HF-R inverter at P_o = 330 W: (a) fixed-phase switches Q_1&Q_2, (b) controlled-phase switches Q_3&Q_4 (50 V/div, 5A/div, 5 μs/div).

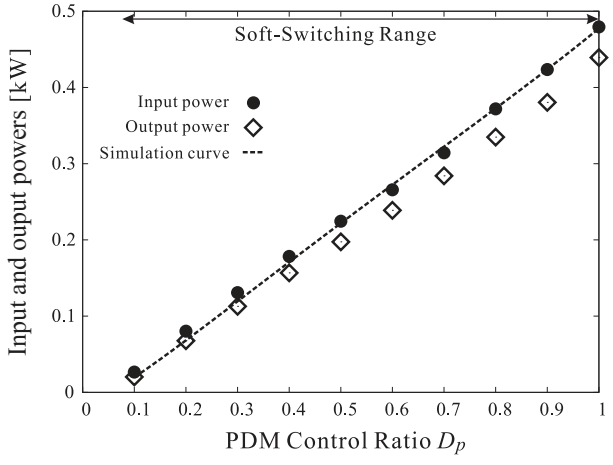

Fig. 34. Experimental characteristics of input and output powers vs. duty cycle curves in asymmetrical PWM.

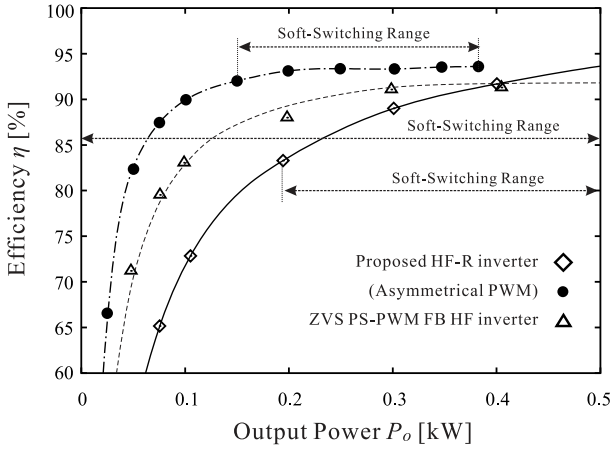

Fig. 35. Actual efficiency vs. output power characteristics in the middle-low output power area.

controlled one unit operation in the proposed HF-R inverter is actually verified for the low output power settings.

V. Conclusions

The novel current phasor-controlled HF-R inverter for the IH applications has been newly proposed in this paper. The operation principle of the proposed HF-R inverter has been explained and the output power regulation performed by the current phasor control has been described by the frequency-domain equivalent circuit-based theoretical analysis. The performances on the soft-switching transitional commutations and the output power regulation in the proposed HF-R inverter have been originally evaluated in an experiment with its laboratory prototype, and its beneficial properties such as a wide-range soft switching operation and high-efficiency power conversion have been actually verified.

The efficiency deteriorates under the conditions of low output powers because the cross current and its relevant reactive power increase between the two half-bridge inverter units when the output power regulation is carried out by only the PS angle control. In order to prevent the efficiency drops, the unit number exchanging from two to one with an asymmetrical PWM has been additionally incorporated into the proposed HF-R inverter prototype operating for the low output power setting. It has been actually demonstrated from the relevant experimental results that more than 20 % efficiency improvement can be achieved for the low output power settings by adopting the PS & asymmetrical PWM dual-mode control scheme.

The comparative investigation between the PS & asymmetrical PWM scheme evaluated herein and another dual mode strategy employing pulse-density-modulation (PDM) [19]–[21] for improving efficiency under the condition of low output power will be one of the next research subjects for the proposed HF-R inverter.

References

[1] H. Sadakata, A. Fujita, S. Sumiyoshi, H. Omori, B. Saha, T. Ahmed and M. Nakaoka, "Latest practical development of triplex series load resonant frequency-operated high frequency inverter for Induction-Heated

Low Resistivity Metal Appliances in Consumer Built-In Cooktops", *Proc. IEEE Applied Power Electronics Conference and Exposition* (IEEE-APEC 2010), Feb. 2010, pp.1825-1832.

[2] J. Jittakort, A. Sangswang, S. Naetiladdanon, C. Koompai, and S. Chudjuarjeen, "A soft switching class D current source inverter for induction heating with non-ferromagnetic load", *Proc. the 14th European Conference on Power Electronic and Applications* (EPE 2011), Aug./Sep. 2011, pp.1-10.

[3] H. Sarnago, O. Lucía, A. Mediano, and J.M. Burdío, "Modulation scheme for improved operation of an RB-IGBT-based resonant inverter applied to domestic induction heating," *IEEE Trans. Ind. Electron.*, vol.60, no.5, pp.2066-2073, May 2013.

[4] C. Carretero, O. Lucía, O. Acero and J.M. Burdío, "Computational modeling of two partly coupled coils supplied by a double half-bridge resonant inverter for induction heating appliances," *IEEE Trans. Ind. Electron.*, vol.60, no.8, pp.3092-3105, Aug. 2013.

[5] I. Hirota, H. Omori, and M. Nakaoka, "Practical evaluations of single ended load-resonant inverter using application-specific IGBT & driver IC for induction-heating appliance," *Proc. IEEE Int. Conf. Power Electronics and Drive Systems* (PEDS), Feb. 1995, vol. 1, pp. 531-537.

[6] O. Lucía, J.M. Burdío, I. Millán, J. Acero, and L.A. Barragán, "Efficiency-oriented design of ZVS Half-bridge series resonant inverter with variable frequency duty cycle control," *IEEE Trans. Power Electron.*, vol.25, no.7, pp.1671-1674, Jul. 2010.

[7] H. Sarnago, M. Saoudi, A. Mediano, D. Puyal, and O. Lucía, "Hybrid full/half wave inverter designed for low cost induction heating appliances, "*Proc. 37th Annual Conference of IEEE Industrial Electronics Society Conference* (IEEE-IECON 2011), Nov. 2011, pp.2539-2544.

[8] B. Saha, S-K. Kwon, N. Ahmed, H. Omori, and M. Nakaoka, "Commercial ac to high frequency ac converter with boost-active clamp bridge single stage ZVS-PWM inverter", *IEEE Trans. Power Electron.*, vol.23, no.1, pp. 412-419, Jan. 2008.

[9] S. Wang, K. Izaki, I. Hirota, H. Yamashita, H. Omori, and M. Nakaoka, "Induction-heated cooking appliance using new quasi-resonant ZVS-PWM inverter with power factor correction," *IEEE Trans. Ind. Appl.*, vol. 34, no. 4, pp. 705-712, Jul./Aug. 1998.

[10] A. Okuno, H. Kawano, J. Sun, M. Kurokawa, A. Kojina, and M. Nakaoka, "Feasible development of soft-switched SIT inverter with load-adaptive frequency-tracking control scheme for induction heating," *IEEE Trans. Ind. Appl.*, vol. 34, no. 4, pp. 713-718, Jul./Aug. 1998.

[11] H. Sugimura, S-K. Kwon, H. Ogiwara, E. Hiraki, and M. Nakaoka, "A new phase-shifted ZVS-PWM controlled full bridge resonant high frequency inverter with auxiliary quasi-resonant commutation circuit", *Proc. the 4th Power Conversion Conference* (PCC), App. 2007, pp.1505-1511.

[12] H. Sugimura, H. Muraoka, T. Ahmed, S. Chandhaket, E. Hiraki, M. Nakaoka, and H. W. Lee, "Dual mode phase-shifted ZVS-PWM series load resonant high-frequency inverter for induction heating super heated steamer," *J. Power Electron.*, vol. 4, no. 3, pp. 138-151, Jul. 2004.

[13] O. Lucía, L.A. Barragán, J.M. Burdío, Ó. Jiménez, D. Navarro, and I. Urriza, "A versatile power electronics test-bench architecture applied to domestic induction heating," *IEEE Trans. Ind. Electron.*, vol.58, no.3, Mar. 2011.

[14] P. Viriya, N. Yongyuth, and K. Matsuse, "Analysis of two continuous control regions of conventional phase shift and transition phase shift for induction heating Inverter under ZVS and NON-ZVS Operation Pichetjamroen," *IEEE Trans. Power Electron.*, vol.23, no.6, pp.2794-2805, Jun. 2008.

[15] J. Jittakort, S. Chudjuarjeen, A. Sangswang, S. Naetiladdanon, and C. Koompai, "A dual output series resonant inverter with improved asymmetrical voltage-cancellation control for induction cooking appliance," *Proc. the 37th Annual Conference of the IEEE Industrial Electronics Society* (IECON 2011), Nov. 2012, pp.2445-2450.

[16] T. Mishima, C. Takami, and M. Nakaoka, "A new ZVS phase-shifted high-frequency resonant inverter incorporating asymmetrical PWM-based unit control for induction heating," *Proc. 38th Annual Conference of the IEEE Industrial Electronics Society* (IEEE-IECON 2012), Oct. 2012, pp.3238-3243.

[17] P. Savary, M. Nakaoka, T. Maruhashi, "A high-frequency resonant inverter using current-vector control scheme and its performance evaluations," *IEEE Trans. Ind. Electron.*, vol.23, no.34, pp. 247-256, May 1987.

[18] D. Czarkowski and M.K. Kazimierczuk, "Phase-controlled series-parallel resonant converter," *IEEE Trans. Power Electron.*, vol.8, no.3, pp.309-319, Jul. 1993.

[19] N.A. Ahmed, "High-frequency soft-switching ac conversion circuit with dual-mode PWM/PDM control strategy for high-power IH applications," *IEEE Trans. Ind. Electron.*, vol.23, no.34, pp. 1440-1448, Apr. 2011.

[20] V. Esteve, E. Sanchis-Kilders, J. Jordan, E.J. Dede, C. Cases, E. Maset, J.B. Ejea, and A. Ferreres, "Improving the efficiency of IGBT series-resonant inverters using pulse density modulation", *IEEE Trans. Ind. Electron.*, vol.58, no.3 pp.979-986, Apr. 2011.

[21] N-J. Park, D-Y. Lee, and D-S. Hyun, "A power-control scheme with constant switching frequency in Class-D inverter for induction-heating jar application," *IEEE Trans. Ind. Electron.*, vol.23, no.3, pp.1252-1260, Jun. 2007.

Tomokazu Mishima (S'00–M'04) received the B.S., M.S., and Ph.D. degree all in electrical engineering from The University of Tokushima, Japan in 1999, 2001, and 2004 respectively. Since 2010, he has been with Kobe University, Hyogo, Japan as an associate professor, and engages in the researches and developments of power electronics circuits and systems. His research interests include soft-switching dc–dc converters, resonant converters, and high frequency inverters for industrial, automotive, renewable and sustainable energy applications.

Dr. Mishima received the Best Paper Award in IEEE-PEDS 2009, and the Best Oral Presentation Award in IEEE-IECON 2012. He serves as an associate editor for the special issue on Transportation Electrification and Vehicle Systems 2013 in IEEE Transaction on Power Electronics Society.

Dr. Mishima is a member of IEEJ (The Institute of Electrical Engineering of Japan), IEICE (The Institute of Electronics, Information and Communication Engineers), and JIPE (The Japan Institute of Power Electronics).

Chikanori Takami received the M.S. degree in the marine engineering from Kobe University, Japan in 2013, where he worked on the research of soft switching power converters including high frequency inverters for induction heatings applied for industrial, commercial and home appliances. Since 2013, he has been with the Welding and Mechatronics Company, Daihen Corporation, Hyogo, Japan, and engages in the research and development of arc welders and the related power converters.

Mr. Takami is a member of IEEJ.

Mutsuo Nakaoka (M'83) received the Ph.D. degree in electrical engineering from Osaka University, Osaka, Japan, in 1981. From 1995 to 2004, he was a professor with the Graduate School of Science and Engineering, Yamaguchi University, Yamaguchi, Japan, and is currently a professor emeritus. Since 2004, he has been a visiting professor with Kyungnam University, Masan, Republic of Korea, and The University of Malaya, Kuala Lumpur, Malaysia since 2010. His research interests include applications and developments of power electronics circuits and systems for industrial electronics and home appliances. From 2001 to 2006, he served as Chairman of the IEEE-IES Japan Chapter.

Prof. Nakaoka received many distinguished paper awards on power electronics such as the 2001 Premium Prize Paper Award from IEE-UK, IEEE-ISIE 2009 Best Paper Award, and IEEE-PEDS 2009 & 2013 Best Paper Awards.

Prof. Nakaoka is a member of IEEJ, IEICE, IEIEJ, and JIPE.